Flight Optimization (*Proceedings of a Colloquium at Univ. of Liege, Belgium*), Pergamon Press, New York, 1969, pp. 157–173.

[15] Robbins, H. M., "Optimality of Intermediate-Thrust Arcs of Rocket Trajectories," *AIAA Journal*, Vol. 3, No. 6, June 1965, pp. 1094–1098.

[16] Moyer, H. G., "Necessary Conditions for Optimal Single Impulse Transfer," *AIAA Journal*, Vol. 4, No. 8, Aug. 1966, pp. 1405–1410.

[17] Contensou, P., "Étude Théorique des Trajectories Optimales dans un Champ de Gravitation. Application au Cas d'un Centre d'Attraction Unique," *Astronautica Acta*, Vol. 8, 1962, pp. 134–150.

[18] Gobetz, F. W., Washington, M., and Edelbaum, T. N., "Minimum Impulse Time-Free Transfer Between Elliptic Orbits," CR-636, Nov. 1966, NASA.

[19] Culp, R. D., "Contensou-Busemann Conditions for Optimal Coplanar Orbit Transfer," *AIAA Journal*, Vol. 5, No. 2, Feb. 1967, pp. 371–372.

[20] Melbourne, W. G., and Sauer, C. G., Jr., "Optimum Interplanetary Rendezvous with Power-Limited Vehicles," *AIAA Journal*, Vol. 1, No. 1, Jan. 1963.

[21] Breakwell, J. V. and Heine, W., "Minimum Impulse Time-Free Transfer Between Neighboring Non-Coplanar Elliptical Orbits with Major Axes Perpendicular to the Line of Nodes," Paper 68-094, AAS/AIAA Astrodynamics Conference, Sept. 3–5, 1968.

APRIL 1971 AIAA JOURNAL VOL. 9, NO. 4

Propagation of Harmonic Waves in Composite Circular Cylindrical Shells. Part II: Numerical Analysis

ANTHONY E. ARMENÀKAS*
Polytechnic Institute of Brooklyn, Brooklyn, N. Y.

The frequency equation for harmonic waves with an arbitrary number of circumferential nodes traveling in composite traction-free circular cylindrical shells established in the first part of this investigation has been programmed for numerical evaluation on an IBM 7094 digital computer. The numerical results obtained are employed in evaluating the effect of the changes of the shell parameters on the frequency and shape of the first few modes of wave propagation. Moreover, the asymptotic limits of the phase velocities for waves having short axial wavelengths are established analytically and verified by the numerical results.

Nomenclature†

R	=	radius of the middle surface of the outer layer
a	=	inner radius of the shell
d	=	outer radius of the shell
b	=	outer radius of the inner layer
$h_1 h_2$	=	thickness of inner and outer layer, respectively
H	=	ratio of the thickness of the inner layer to the thickness of the outer layer
u_x, u_θ, u_r	=	axial, tangential and radial components of displacement
$\zeta = h_2/L$	=	nondimensionalized wave number in the axial direction
L	=	axial half-wave length
n	=	number of circumferential waves
ω	=	circular frequency
v_{1i}, v_{2i}	=	velocity of propagation of dilatational and of shear waves, in an infinite medium, respectively
$\Omega_i = \omega h_2/\pi v_{2i}$	=	nondimensionalized frequency
E_i, μ_i	=	Young's modulus and shear modulus, respectively
$\rho = \rho_1/\rho_2$	=	density ratio
$\mu = \mu_1/\mu_2$	=	stiffness ratio
$\alpha_i \beta_i$	=	radial wavenumbers, see Eq. (1)
$\bar{\alpha}_i \bar{\beta}_i$	=	modulus of α_i and β_i, respectively

Received November 19, 1969; revision received June 29, 1970. This investigation was supported by the U.S. Office of Naval Research under contract number 839 (40) FBM with the Polytechnic Institute of Brooklyn. The author wishes to acknowledge A. Kohen's and J. Housner's assistance with the computations.

* Professor of Applied Mechanics, Department of Aerospace Engineering and Applied Mechanics. Associate Fellow AIAA.

† The subscript i assumes the values 1 or 2, depending on whether reference is made to the inner layer or outer layer, respectively.

Introduction

IN the first part of this investigation,[1] the frequency equation has been derived for harmonic waves with an arbitrary number of circumferential nodes traveling in composite traction-free circular cylindrical shells. The composite shells consist of two-concentric circular, cylindrical shells bonded at their interface. For given physical and geometric properties of the shell, the frequency equation constitutes a transcendental relation between the nondimensionalized frequency $\Omega_i = (\omega h_i \rho_i^{1/2}/\pi \mu_i^{1/2})$ $(i = 1,2)$ the nondimensionalized wave number $\zeta = h_2/L$ and the number of circumferential waves n. For any chosen value of n and h_2/L, the frequency equation yields an infinite number of values of Ω_i.

In the second part of this investigation, the frequency equation has been programed for numerical evaluation on an IBM 7094 digital computer. The program computes the value of the determinant at a specified initial value of Ω_2 and at values of Ω_2 incremented by $\Delta\Omega_2$. A root is indicated by a change of sign of the determinant between two successive values $\bar{\Omega}_2$ and $\bar{\Omega}_2 + \Delta\bar{\Omega}_2$. The increment is then halved, and commencing with $\bar{\Omega}_2$, the process is repeated until the root is established to the desired accuracy. Subsequently, starting with a new value of Ω_2 obtained by adding a specified increment to the established root, the program continues to establish any number of successive roots desired. The program can also evaluate the amplitude of the displacement components u_r and u_z for axisymmetric nontorsional motion at a specified number of points across the thickness of the shell.

The numerical results obtained are employed in evaluating the effect of the changes of the shell parameters on the frequency and shape of the first few modes of wave propagation. Moreover, the asymptotic behavior of the frequency lines

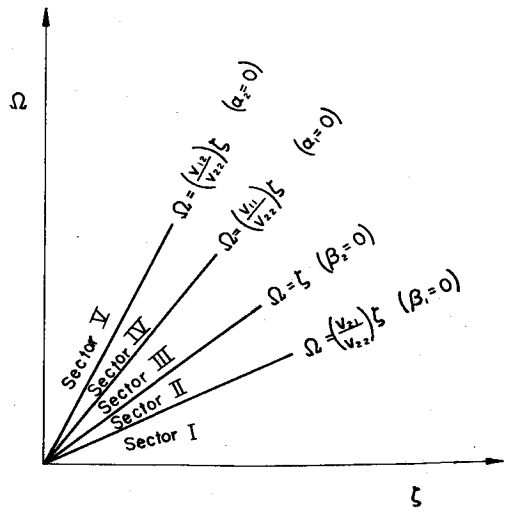

Fig. 1 Ω-ζ plane showing sector lines for the case $v_{12} > v_{11} > v_{22} > v_{21}$.

has been investigated analytically and verified by the numerical results. It is shown, that the phase velocity of at most the first two modes, approaches asymptotically that of the Rayleigh waves in the two materials, and that the phase velocity of one mode (the second or third), may approach asymptotically that of Stoneley waves traveling at the interface of the two materials. All other modes approach asymptotically the least shear wave velocity in the two materials.

Asymptotic Limits of the Phase Velocity of Waves Having Short Axial Wavelengths

The frequency equation established in Ref. (1) is a 12 × 12 determinant whose terms are polynomials involving Bessel functions with arguments which are multiples of the radial wave numbers α_i and β_i, defined by Eq. (11), in Part 1. These radial wave numbers may be rewritten in terms of the nondimensionalized frequency Ω_2 and wave number ζ as

$$(\alpha_i)^2 = (\pi\zeta/h_2)^2[(\Omega_2/\zeta)^2(v_{22}/v_{1i})^2 - 1]$$
$$(\beta_i)^2 = (\pi\zeta/h_2)^2[(\Omega_2/\zeta)^2(v_{22}/v_{2i})^2 - 1] \quad (1)$$

The radial wave numbers may be either real or imaginary, depending upon the relative magnitude of Ω_2 and ζ. If α_i or β_i is real, the corresponding Bessel functions involved in the terms of the frequency determinant are J_n and Y_n functions. If α_i or β_i is imaginary, the corresponding Bessel functions are I_n and K_n functions. It is evident, therefore, that the character of the frequency equation will change when α_i or β_i changes from real to imaginary, or vice versa. Thus, the Ω_2-ζ plane may be divided into five sectors (Fig. 1), by the following sector lines

$$\alpha_i = 0 \; \beta_i = 0 \; (i = 1,2) \quad (2)$$

In each sector, the frequency lines are derived from the same frequency equation.

In the Ω_2-ζ plane, the slope of a line from the origin to any point on a frequency line is the phase velocity, nondimensionalized with respect to v_{22}, whereas, the slope of the tangent at any point on the frequency line is proportional to the group velocity. As the axial wave-length decreases, the phase velocity ($v/v_{22} = \Omega_2/\zeta$) of the various modes approaches asymptotically certain finite limits. Thus, the arguments of the Bessel functions increase as ζ increases and, consequently, the Hankel approximations of the Bessel functions of large arguments may be employed.

$$J_n(z) = \left(\frac{2}{\pi z}\right)^{1/2} \cos\left(z - \frac{\pi}{4} - \frac{n\pi}{2}\right) \quad I_n(z) = (2nz)^{1/2}e^z$$
$$Y_n(z) = \left(\frac{2}{\pi z}\right)^{1/2} \sin\left(z - \frac{\pi}{4} - \frac{n\pi}{2}\right) \quad K_n(z) = \left(\frac{\pi}{2z}\right)^{1/2} e^{-z} \quad (3)$$

For waves with small axial wavelengths, as compared to their circumferential wavelength ($\zeta \gg h_2 n/2\pi R$), the effect of the latter on the frequency is negligible. It can be shown, that as $\zeta \to \infty$ the frequency determinant [Eq. (20) Part I] decomposes into the product of two determinants

$$D_1 \times D_3 = 0 \quad (4)$$

where D_1 and D_3 are given in Part I by Eqs. (24) and (25). They are the frequency determinants of axisymmetric nontorsional and torsional modes, respectively. Thus, as $\zeta \to \infty$ some of the frequency lines of the nonaxisymmetric modes ($n \neq 0$) will converge to those of the axisymmetric nontorsional modes, whereas, the others will converge to those of the torsional modes.

In can be shown, that as $\zeta \to \infty$, all frequency lines are in Sectors I and II. Consequently, it is necessary to examine equations $D_1 = 0$ and $D_3 = 0$ solely in these two sectors in order to establish the limiting values of the phase velocity of the various modes. Sector I is bounded by the sector line $\beta_1 = 0$ if $v_{22} > v_{21}$, or by the sector line $\beta_2 = 0$ if $v_{21} > v_{22}$. In this sector, for large values of ζ, Eq. $D_3 = 0$, reduces to

$$\mu\beta_1^2\bar{\beta}_2 + \bar{\beta}_1\beta_2^2 = 0 \quad (5)$$

This equation cannot be satisfied for positive values of μ, consequently, it is concluded that for large values of ζ the frequency equation $D_3 = 0$ does not have any real roots in Sector I.

For large values of ζ, equation $D_1 = 0$ degenerates in Sector I into the product of three determinants

$$D_1 = D_5^{(1)} \times D_6 \times D_5^{(2)} = 0 \quad (6)$$

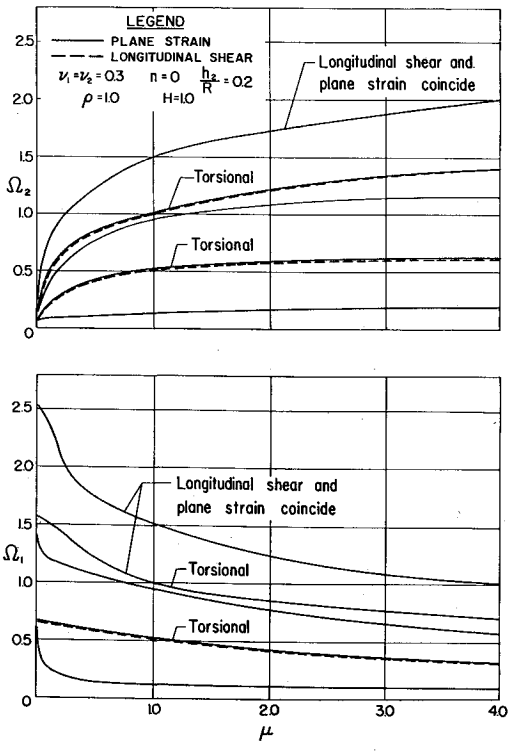

Fig. 2 Cutoff frequencies as functions of the stiffness ratio.

where

$$D_5^{(1)} = \begin{vmatrix} \bar{C}_{12} & \bar{C}_{14} \\ \bar{C}_{32} & \bar{C}_{34} \end{vmatrix} \quad D_5^{(2)} = \begin{vmatrix} \bar{C}_{47} & \bar{C}_{49} \\ \bar{C}_{67} & \bar{C}_{69} \end{vmatrix} \tag{7}$$

$$D_6 = \begin{vmatrix} \bar{C}_{71} & \bar{C}_{73} & \bar{C}_{78} & \bar{C}_{7,10} \\ \bar{C}_{91} & \bar{C}_{93} & \bar{C}_{98} & \bar{C}_{9,10} \\ \bar{C}_{10,1} & \bar{C}_{10,3} & \bar{C}_{10,8} & \bar{C}_{10,10} \\ \bar{C}_{12,1} & \bar{C}_{12,3} & \bar{C}_{12,8} & \bar{C}_{12,10} \end{vmatrix} \tag{8}$$

$\bar{C}_{ij}$ are the limits as $\zeta \to \infty$ evaluated in Sector I, of the terms C_{ij} defined by Eq. (20) in Part I.

Equations $D_5^{(1)} = 0$ and $D_5^{(2)} = 0$ are the frequency equations for Rayleigh surface waves traveling in a semi-infinite elastic body, having the mechanical properties of the inner or outer layer, respectively. The velocity of the Rayleigh waves v_{Ri} is always less than the shear wave velocity v_{2i} in a material. Consequently, if $v_{21} > v_{22}$ the Rayleigh wave frequency line for the outer material is in Sector I, whereas, the Rayleigh wave frequency line for the inner material may or may not be in Sector I. Thus for this case equation $D_5^{(1)} = 0$ has an acceptable solution only if $v_{22} > v_{R1}$. Similarly if $v_{22} > v_{21}$, the Rayleigh wave frequency line for the inner material is in Sector I whereas that of the outer material may or may not be in Sector I. Consequently, in this case equation $D_5^{(2)} = 0$ has an acceptable solution only if $v_{21} > v_{R2}$.

Equation $D_6 = 0$ is the frequency equation for Stoneley waves at the interface of the two layers. This frequency equation has been investigated extensively in Refs. 3 and 4. It has been established that it has real roots only for certain values of the ratio of the densities and stiffnesses of the two materials.

For the Case $D_5^{(1)} = 0$, the motion is confined to the inner layer of the shell and the displacement field decays exponentially from its inner surface. For the case $D_5^{(2)} = 0$, the motion is confined in the outer layer of the shell and the displacement field decays exponentially from its outer surface. For the case $D_6 = 0$, the displacement field decays exponentially, from the interface.

For shells with $v_{21} < v_{22}$ Sector II is separated from Sector I by the line $\beta_1 = 0(\Omega_2/\zeta = v_{21}/v_{22} < 1)$. For large values of ζ, in this case, the frequency equation $D_3 = 0$ reduces in Sector II to

$$\tan(a - b)\beta_1 = \frac{[1 - (\Omega_2/\zeta)^2]^{1/2}}{\mu[(\Omega_2/\zeta)^2(v_{22}/v_{21})^2 - 1]^{1/2}} \tag{9}$$

As $\zeta \to \infty$, this relation reduces to

$$\Omega_2/\zeta = v_{21}/v_{22} \tag{10}$$

For this case, the motion is oscillatory in the inner layer and decays exponentially in the outer layer.

For shells with $v_{21} < v_{22}$ for large values of ζ the frequency equation $D_1 = 0$, reduces in Sector II to the product of the following two determinants

$$D_1 = D_5^{(2)} \times D_7 \tag{11}$$

where $D_5^{(2)}$ is the frequency determinant [Eq. (7)] for Rayleigh waves in the material of the outer layer, whereas, D_7 is given by

$$D_7 = \begin{vmatrix} 0 & \bar{C}_{12} & \bar{C}_{13} & \bar{C}_{14} & 0 & 0 \\ 0 & \bar{C}_{32} & \bar{C}_{33} & \bar{C}_{34} & 0 & 0 \\ \bar{C}_{71} & 0 & \bar{C}_{73} & \bar{C}_{74} & \bar{C}_{78} & \bar{C}_{7,10} \\ \bar{C}_{91} & 0 & \bar{C}_{93} & \bar{C}_{94} & \bar{C}_{98} & \bar{C}_{9,10} \\ \bar{C}_{10,1} & 0 & \bar{C}_{10,3} & \bar{C}_{10,4} & \bar{C}_{10,8} & \bar{C}_{10,10} \\ \bar{C}_{12,1} & 0 & \bar{C}_{12,3} & \bar{C}_{12,4} & \bar{C}_{12,8} & \bar{C}_{12,10} \end{vmatrix} \tag{12}$$

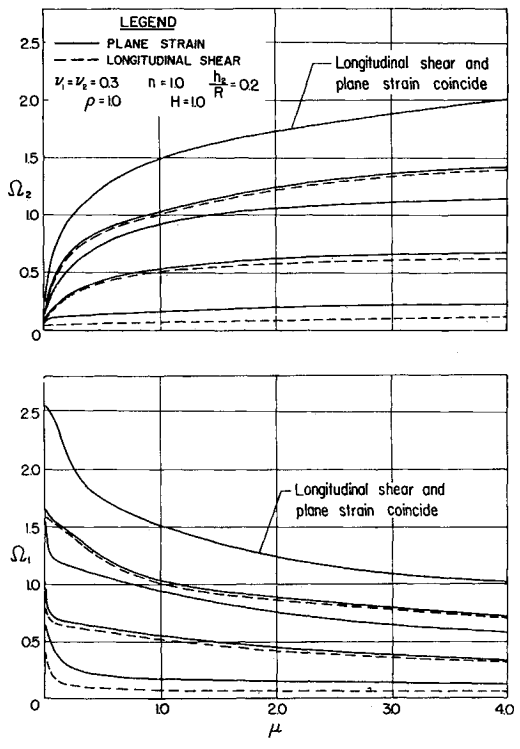

Fig. 3 Cutoff frequencies as functions of the stiffness ratio.

where $\bar{C}_{ij}$ are the limits as $\zeta \to \infty$, evaluated in Sector II, of the terms C_{ij} defined by Eq. (20) in Part I. It can be shown that in the limit as $\zeta \to \infty$, the frequency equation (12) yields

$$\Omega_2/\zeta = v_{21}/v_{22} \tag{13}$$

For this case the motion is oscillatory in the inner layer and decays exponentially in the outer layer.

For shells with $v_{21} > v_{22}$ it can be shown that as $\zeta \to \infty$ the frequency equation $D_3 = 0$ reduces in Sector II to

$$\Omega_2/\zeta = 1 \tag{14}$$

For this case, the motion is oscillatory in the outer layer and increases exponentially with the radius in the inner layer.

For shells with $v_{21} > v_{22}$ the frequency equation $D_1 = 0$ reduces for large values of ζ to the product of two determinants

$$D_1 = D_7 \times D_5^{(1)} \tag{15}$$

$D_5^{(1)}$ is the frequency determinant for Rayleigh waves in the material of the inner layer [Eq. (7)] whereas D_7 is defined by Eq. (13). In the limit as $\zeta \to \infty$ the frequency equation $D_7 = 0$ reduces to

$$\Omega_2/\zeta = 1 \tag{16}$$

For this case, the motion is oscillatory in the outer layer, and increases exponentially in the inner layer.

Thus, it may be concluded that for very large axial wave numbers, the phase velocity of the nonaxisymmetric waves approaches asymptotically the same limiting values as those of the axisymmetric waves. For shells with $v_{22} > v_{21}$, the phase velocity of the first mode approaches asymptotically the Rayleigh velocity in the inner layer; if in addition $v_{21} > v_{R2}$, the phase velocity of the second mode approaches asymptotically that of the Rayleigh waves in the outer layer, whereas for shells with $v_{21} < v_{R2}$ the phase velocity of the second mode may approach that of the Stoneley waves if the physical properties of the two materials are such that a Stoneley wave can be sustained at their interface; otherwise, the phase velocity of the second mode will approach that of

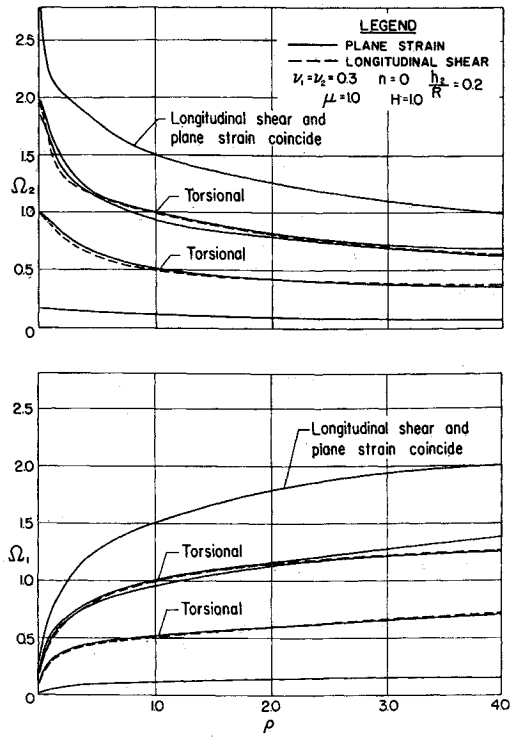

Fig. 4 Cutoff frequencies as functions of the density ratio.

shear waves in the material of the inner layer. The phase velocity of the third mode will approach that of the shear waves in the material of the inner layer except possibly for shells with $v_{21} > v_{R2}$. In this case, it may approach the phase velocity of the Stoneley waves if such waves can be sustained at the interface of the two materials. The phase velocity of all higher modes will approach asymptotically that of the shear waves in the material of the inner layer. An analogous situation exists for shells with $v_{21} > v_{22}$.

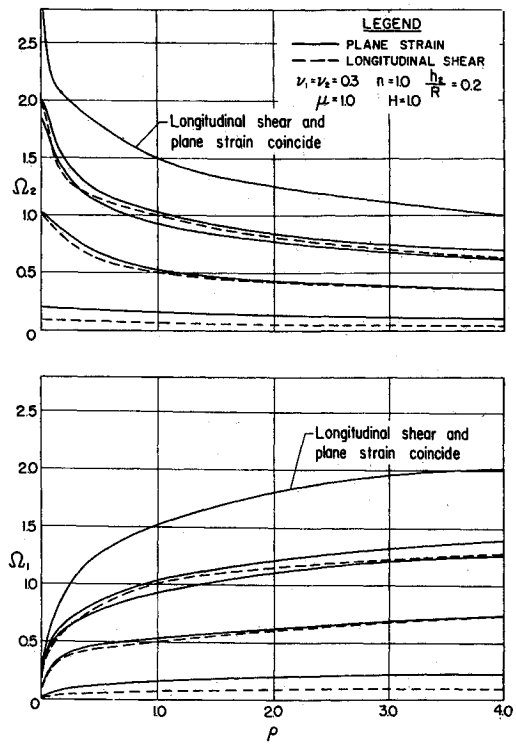

Fig. 5 Cutoff frequencies as a function of the density ratio.

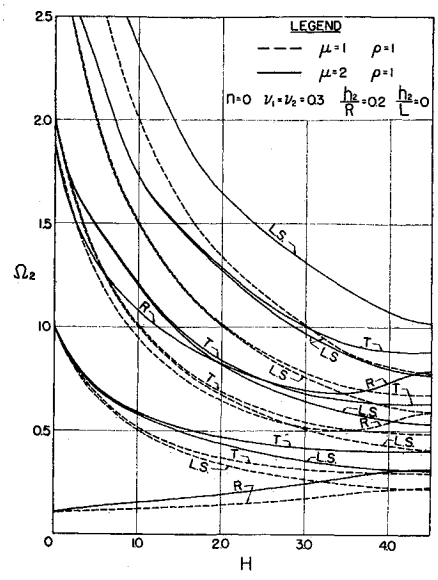

Fig. 6 Variation of the cutoff frequencies as functions of the thickness ratio.

Discussion of the Numerical Results

The frequency equation has been evaluated for $n = 0,1$ for shells having geometries specified by $h_2/R = 0.2$; h_2 being the thickness of the outer layer, R being the radius of the center line to the outer layer. In Part I, it was established that when the motion is independent of the axial coordinate ($h_2/L = 0$), the thickness shear modes ($u_r = u_\theta = 0$) and the plane strain modes ($u_x = 0$) exist uncoupled.[5] Moreover, in the case of axisymmetric motion independent of the axial coordinate ($n = 0, h_2/L = 0$), the radial and tangential modes also exist uncoupled.

The effect of the stiffness ratio ($\mu = \mu_1/\mu_2$) and the density ratio ($\rho = \rho_1/\rho_2$) on the cutoff frequency of the first six modes is illustrated in Figs. 2 and 3 and 4 and 5, respectively. The graphs of Ω_1 vs μ or ρ illustrate the influence on the frequency of the stiffness or density of the outer layer, whereas the graphs of Ω_2 vs μ or ρ illustrate the influence on the frequency of the stiffness or density of the inner layer. As anticipated, Ω_2 increases as μ increases, and decreases as ρ increases, whereas Ω_1 decreases as μ increases, and increases as ρ increases. This effect is more pronounced in higher modes.

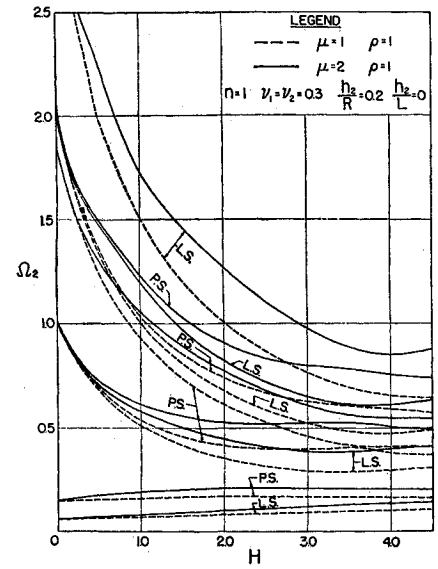

Fig. 7 Variation of the cutoff frequencies as functions of the thickness ratio.

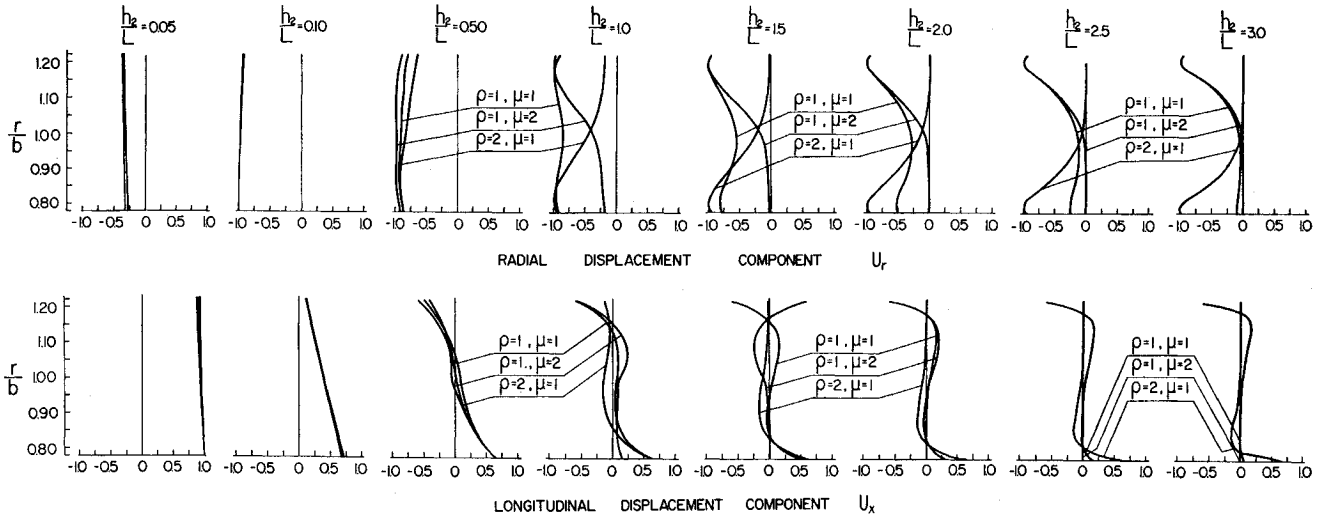

Fig. 8 Shape of the first axisymmetric nontorsional mode.

The effect of the geometry of the shell on the cutoff frequency of the first six modes is illustrated in Figs. 6–7, wherein the frequency Ω_2 is plotted as a function of the thickness ratio $H = h_1/h_2$. In these graphs, $H = 0$ denotes a shell of one material, with thickness h_2, whereas higher values of H indicate a composite shell with the thickness of its inner layer increasing as H increases until when $H = 4.5$, a composite rod is denoted. As H increases, both the mass of the shell and its structural rigidity increase. An increase of the mass will tend to decrease the frequency, whereas an increase of the rigidity will tend to increase it. Thus, the frequency will increase or decrease with H, depending upon whether the effect of the increase of the rigidity, or the effect of the increase of mass is more predominant. At infinite axial wavelength, the first axisymmetric mode with nonzero frequency is a breathing mode, involving radial motion ($u_\theta = u_x = 0$). The frequency of this mode increases monotonically with H. This implies that the frequency of this mode is affected more by the increase of the rigidity of the shell than by the increase of its mass. The cutoff frequency of the next axisymmetric, radial mode, however, decreases as H increases, except for large values of H. The cutoff frequency of the other modes in shells having small values of H decreases abruptly as H increases. However, for higher values of H the cutoff frequency decreases at a slower rate as H increases.

For very large axial wavelengths, ($h_2/L < 0.05$) the first axisymmetric nontorsional mode involves predominantly uniform extension (Fig. 8). However, as the wavelength decreases, the radial component of motion increases. For short axial wavelengths, the phase velocity of the first axisymmetric nontorsional mode and the first flexural mode ($n = 1$) approaches, for shells made of one material, the phase velocity of Rayleigh waves in the material. The displacement decreases exponentially from the outer surface of the shell. For short axial wavelengths, the phase velocity of the first axisymmetric nontorsional mode and of the first flexural mode ($n = 1$) approaches, for composite shells with $\mu = 1$, $\rho = 2$, the phase velocity of Rayleigh waves in the material of the inner shell (Figs. 9, 10), and for composite shells with $\mu = 2$, $\rho = 1$ the phase velocity of Rayleigh waves in the material of the outer shell (Figs. 11, 12). The motion is predominantly radial concentrated in the inner layer in the case of shells with $\mu = 1$, $\rho = 2$, and in the outer layer in the case of shells with $\mu = 2$, $\rho = 1$.

For shells made of one material, the first torsional mode is nondispersive with a phase velocity Ω_2/ζ. For composite shells, however, this mode is slightly dispersive. For short axial wavelengths, its phase velocity approaches, for shells with $\mu = 1$, $\rho = 2$, the velocity of shear waves ($\beta_1 = 0$) in the material of the inner shell, whereas, for shells with $\mu = 2$, $\rho = 1$, it approaches the velocity of shear waves ($\beta_2 = 0$) in the material of the outer shell.

At infinite wavelength, the second axisymmetric nontorsional mode involves radial motion, constant along the thickness of the shell (breathing). As the wavelength decreases, the motion becomes less uniform and has both radial and extensional components. For very short axial wavelengths, for shells made of one material the phase velocity of the second mode approaches that of Rayleigh waves. For composite shells with $\mu = 1$, $\rho = 2$ and $\mu = 2$, $\rho = 1$, the phase velocity of the second mode approaches the least shear wave velocity in the two materials. For composite shells with $\mu = 1$, $\rho = 2$, the motion is concentrated

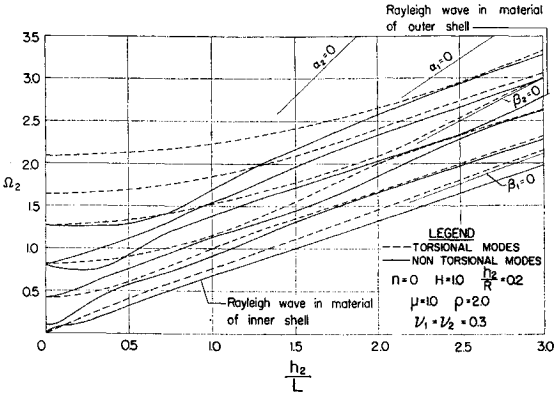

Fig. 9 Frequency spectrum of axisymmetric modes.

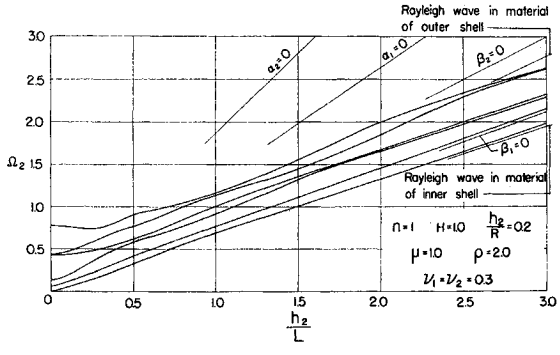

Fig. 10 Frequency spectrum of flexural ($n = 1$) modes.

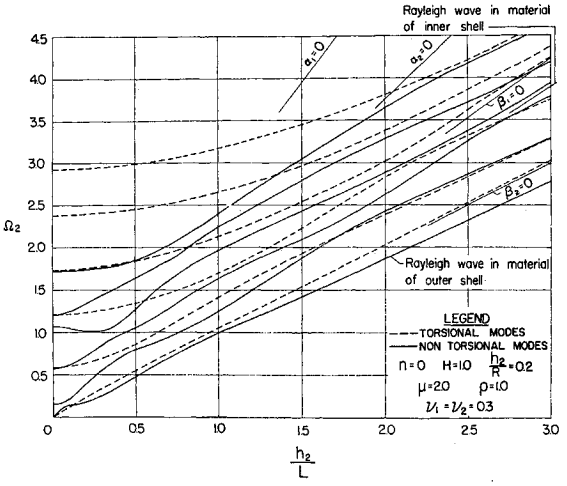

Fig. 11 Frequency spectrum of axisymmetric modes.

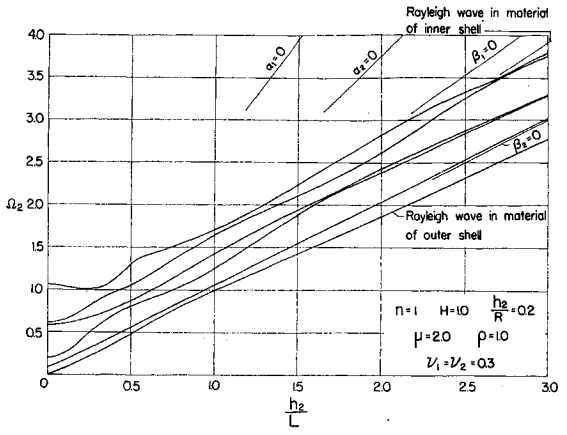

Fig. 12 Frequency spectrum of flexural (n = 1) modes.

in the inner layer, whereas, for shells with $\mu = 2$, $\rho = 1$, the motion is concentrated in the outer layer (Fig. 13).

At infinite wavelength, the third axisymmetric nontorsional mode involves simple thickness shear motion with one nodal cylinder. At finite wavelengths, the motion involves both longitudinal and radial components of displacement. For very short wavelengths, the motion becomes predominantly radial, concentrated for shells with $\mu = 2$, $\rho = 1$, in the outer layer, and, for shells with $\mu = 1$, $\rho = 2$, in the inner layer (Fig. 14).

The frequency lines of the third and higher modes, apparently, pair one torsional and one nontorsional mode, and

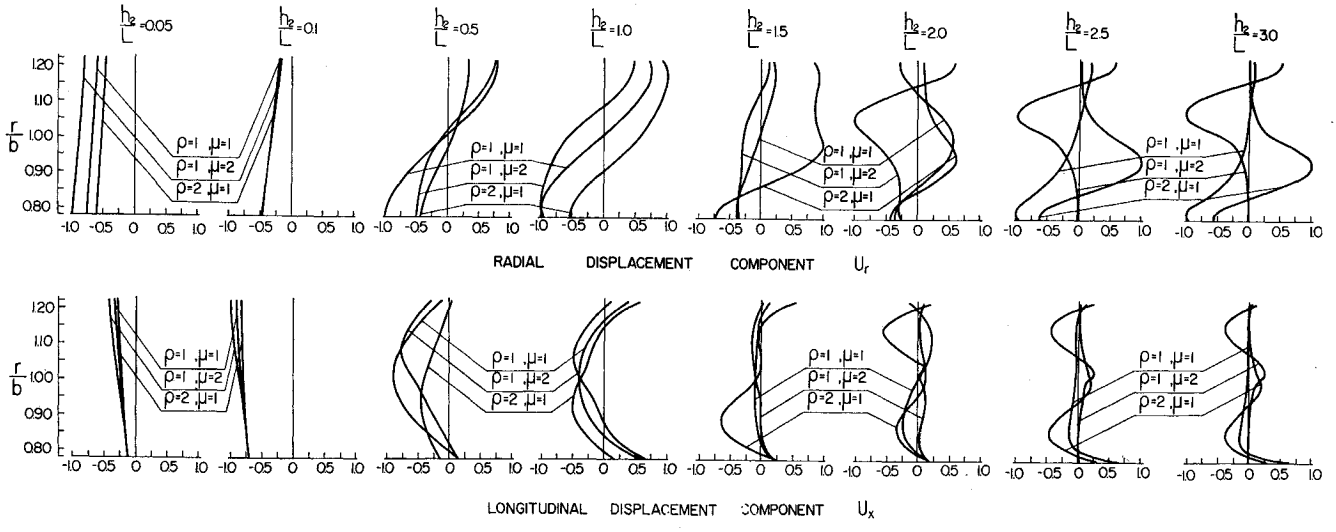

Fig. 13 Shape of the second axisymmetric nontorsional mode.

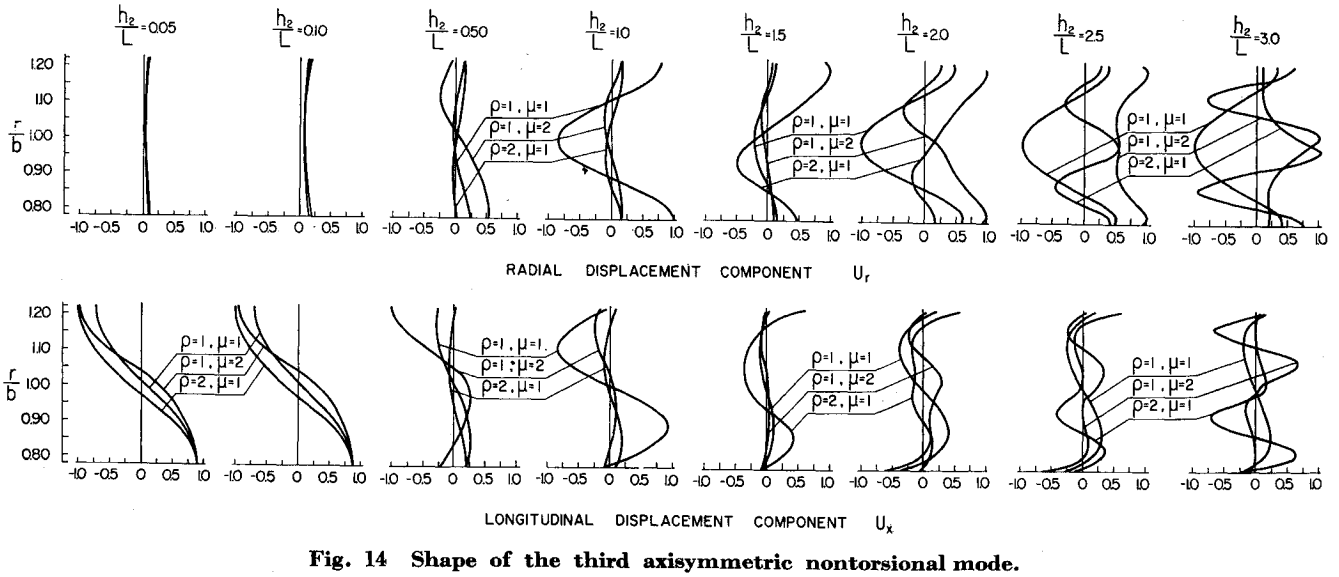

Fig. 14 Shape of the third axisymmetric nontorsional mode.

for short axial wavelengths become parallel to the sector line ($\beta_1 = 0$) with the least slope. For shells with $\mu = 1$, $\rho = 2$, the frequency lines of the third and fourth axisymmetric nontorsional modes become parallel to the frequency line of the Rayleigh waves in the material of the outer shell, prior to becoming parallel to the sector line $\beta_2 = 0$ (Fig. 9), whereas, in the case of shells with $\mu = 2$, $\rho = 1$, they become parallel to the frequency line of the Rayleigh waves in the material of the inner shell prior to becoming parallel to the sector line $\beta_1 = 0$.

The frequency lines of the fourth, fifth and sixth torsional modes and the fifth and sixth nontorsional modes for shells with $\mu = 1$, $\rho = 2$, become parallel to the sector line $\beta_2 = 0$ before, for higher values of ζ not included in the figures, becoming parallel to the sector line $\beta_1 = 0$. Analogous behavior is observed for shells with $\mu = 2$, $\rho = 1$.

The behavior of the frequency lines of the flexural modes ($n \geq 1$,) is similar to that of the axisymmetric modes, except that they do not exhibit the tendency of becoming parallel to the sector line $\beta_i = 0$, with the greatest slope. For $n = 1$, for large axial wavelengths the first mode is essentially a uniform translation of the entire cross section, the second mode involves essentially longitudinal shear motion, whereas the third mode is associated with predominantly radial motion (breathing). The three lowest flexural modes are those contained in the bending shell theories, wherein the radial component of the displacement is assumed constant across the thickness of the shell and the tangential and axial components are assumed to vary linearly with the thickness coordinate.

References

[1] Armenàkas, A. E., "Propagation of Harmonic Waves in Composite Circular Cylindrical Shells, I: Theoretical Investigation," *AIAA Journal*, Vol. 5, No. 4, April 1967, pp. 740–744.

[2] Stoneley, R., "Elastic Waves at the Surface of Separation of Two Solids," *Proceedings of the Royal Society*, Vol. A 106, 1924, pp. 416–428.

[3] Scholte, J. G., "The Range of Existence of Rayleigh and Stoneley Waves," *Monthly Notices Royal Astronomical Society Geophysic Supplement*, Vol. 5, 1947, pp. 120–126.

[4] Sezawa, K. and Kanai, K. "The Range of Possible Existence of Stoneley Waves," *Bulletin of Earthquakes Research Institute*, Vol. 17, 1938, pp. 1–8.

[5] Karlsson, T. and Ball, R. E., "Exact Plane Strain Vibrations of Composite Hollow Cylinders: Comparison with Approximate Theories," *AIAA Journal*, Vol. 4, No. 1, Jan. 1966, pp. 179–181.

APRIL 1971 AIAA JOURNAL VOL. 9, NO. 4

A Study of the Buckling of Laminated Composite Plates

T. P. KICHER* AND J. F. MANDELL†

Case Western Reserve University, Cleveland, Ohio

Buckling loads are determined for approximately square, simply supported plates of the following materials: aluminum, steel, glass fiber reinforced composites and graphite fiber reinforced composites. The plates are subjected to a uniformly distributed compressive edge load in one direction only. Buckling loads are determined from experimental load vs transverse displacement data using a Southwell Plot. Analytical buckling loads for elastically balanced plates are determined from classical plate theory. For plates with bending-membrane coupling effects, the reduced flexural stiffness method is utilized to find eigenvalue upper bounds. The effectiveness and consequences of using the reduced flexural stiffness method are examined.

Nomenclature

a,b	=	planform dimensions of the plate
A,B,D	=	element matrices of the constituitive equation
A^*,B^*,D^*	=	element matrices of the partial inverse form of the constituitive equations
(e)	=	vector of strain components (e_x,e_y,e_{xy})
(κ)	=	vector of curvature components $(\kappa_x,\kappa_y,\kappa_{xz})$
L_1,L_2,L_3,L_4	=	differential operators
m,n	=	buckling wave numbers
(M)	=	vector of mement resultants (M_x,M_y,M_{xy})
(N)	=	vector of force resultants (N_x,N_y,N_{xy})
P	=	total axial load
u,v,w	=	displacements
V	=	strain energy of deformation
x,y,z	=	coordinate variables
Δ	=	maximum transverse displacement
θ	=	orientation of the fibers in a single ply referenced to the x axis (Fig. 1)
Π	=	generalized potential function
ϕ	=	airy stress function

Subscripts

cr	=	critical or buckling value
o	=	prebuckling
$,$	=	differentiation with respect to the variables which follow the comma

Superscripts

$\sim$	=	quantities associated with buckling
$-$	=	quantities imposed at the boundaries

Received January 20, 1969; revision received November 2, 1970. Sponsored by the Advanced Research Projects Agency, through a contract with the Air Force Materials Laboratory. Based on a paper presented at the AIAA/ASME 10th Structures, Structural Dynamics and Materials Conference, New Orleans, La., April 14–16, 1969.

* Associate Professor of Engineering. Member AIAA.

† Graduate Student, now at MIT.